Supporting Information

Apically Co-nanoparticles-wrapped nitrogen-doped carbon nanotubes from a single-source MOF for efficient oxygen reduction

Lin Ma,[a] Rui Wang,[a] Ya-Hui Li,[a] Xiao-Fei Liu,[a] Qing-Qing Zhang,[a] Xi-Yan Dong[a,b] and Shuang-Quan Zang,*[a]

[a] College of Chemistry and Molecular Engineering, Zhengzhou University, Zhengzhou 450001, China
[b] College of Chemistry and Chemical Engineering Henan Polytechnic University Jiaozuo 454000, China

Author for correspondence: **Prof. S.-Q. Zang**

EXPERIMENTAL SECTION

Materials.

All the chemicals in this work, including cobalt nitrate trihydrate ($Co(NO_3)_2 \cdot 3H_2O$, 99%), sodium dicyanamide (Na(dca), 99%), pyrazine ($C_4H_4N_2$,99%) and commercial Pt/C (Pt 20 wt.%) were obtained commercially and used without further purification. All the solvents used were of analytical grade.

Instrumentation and Measurements

X-ray diffraction (XRD) patterns of the compounds were recorded on a Rigaku B/Max-RB X-ray diffractometer with Cu Ka radiation (λ = 1.5418 Å). FT-IR spectra were measured on a Nexus 870 FT-IR spectrometer from KBr pellets as the sample matrix. X-ray photoelectron spectroscopy (XPS) measurements were performed using ESCALAB 250 system (Thermo Electron) with a Al Kα (300 W) X-ray resource. Field-emission scanning electron microscopy (FESEM) measurement was carried out using Zeiss Sigma 500, the catalysts were dispersed in ethanol by ultrasonication for 30 minutes, and dripped onto the conducting substrates and then dried under ambient conditions for SEM measurements. The transmission electron microscopy (TEM) and high resolution transmission electron microscopy (HRTEM) images were obtained in FEI Tecnai G2 F20 S-TWIN electron microscope at an accelerating voltage of 200 kV. Raman spectra were recorded on a LabRam HR Evolution with excitation from the 532 nm line of an Ar-ion laser. Nitrogen sorption isotherms were measured at liquid nitrogen temperature (77 K) by using automatic volumetric adsorption equipment (Belsorp Max) after a degassed process at 100 ℃ for 12 h. Specific surface areas were obtained by using the Brunauer–Emmet–Teller (BET) model, pore size distributions were simulated by the nonlocal density functional theory (NLDFT) model, and the pore volumes were calculated from the amount adsorbed at P/P_0=0.99.

Synthesis of Co-MOF

$Co(dca)_2pyz$ used in this work was prepared by using the improved method according to the literature.[35] In a typical procedure, 0.38 g $Co(NO_3)_2 \cdot 3H_2O$ was dissolved in 20 mL hot H_2O to form aqueous solution A. 0.2 g Na(dca) and 0.096 pyrazine were dissolved in 20 mL hot H_2O to form aqueous solution B. Then solution A and solution B were mixed and vigorously stirred for 30 min at ambient temperature to form the pink precipitates. After collected by centrifugation and washed with water and ethanol several times, the as-obtained precipitates were dried at 60 ℃ overnight.

Synthesis of Co@BNCNTs Catalysts

To prepare Co@BNCNTs, the as-synthesized $Co(dca)_2pyz$ are dispersed in a quartz boat, heated to different temperature (700, 800, 900, 1000 ℃) and maintained for 3 h in a tube furnace with a heating rate of 10° per min under a flowing N_2. After that, the furnace is cooled down to room temperature naturally. Then the as-obtained black composites were added into 30 mL 1 M H_2SO_4 and 1 M KOH, and this solution was sonicated for 30 min. The sample of powder obtained by extraction filtration was washed by deionized water and ethanol several times respectively, and dried in a vacuum oven at 60 ℃ for 12 h. A series of samples obtained at different temperatures were named as Co@BNCNTs-700 (700 ℃), Co@BNCNTs-800 (800 ℃), Co@BNCNTs-900 (900 ℃) and Co@BNCNTs-1000 (1000 ℃).

Electrochemical measurements

For ORR, electrochemical measurements were conducted on a typical three-electrode system using a pine electrochemical workstation equipped (Wavedrive 20) with MSR electrode rotator (Pine Instrument Co.). An Ag/AgCl (KCl, saturated) electrode and Pt wire were used as the reference and counter electrodes, respectively. A glassy carbon electrode (GCE) coated with the as-prepared catalysts ink was used as the

working electrode. The glassy carbon electrode was polished using 0.05 um alumina powder before surface coating, followed by sonication in dilute nitric acid solution, water, and ethanol respectively, and then allowed to dry at room temperature. The well-dispersed catalyst ink was prepared by dispersing 2 mg of catalyst in 320 μL of solution containing 150 μL of isopropanol, 150 μL of water and 20 μL of 5 wt.% Nafion solution followed by ultrasonication for 30 min. Cyclic voltammetry (CV) measurements were carried out in N_2 - or O_2 - saturated 0.1 M KOH solution at a scan rate of 20 mV s^{-1}. Rotating disk electrode (RDE) measurements were performed by linear sweep voltammetry at a sweep rate of 5 mV s^{-1} with various rotating speeds ranging from 400 to 2500 rpm. 10 μL of the catalyst ink was pipetted onto the RDE surface (5 mm in diameter, S = 0.1962 cm^2) and Rotating Ring-Disk electrode (RRDE) surface (5.61 mm in diameter, S = 0.2470 cm^2) using a micropipettor and then dried at ambient temperature. The loading amount of catalyst is 0.3 mg cm^{-2} on the GCE. All potentials were converted to the reversible hydrogen electrode (RHE): E (RHE) = E (Ag/AgCl) + 0.198 + 0.059 × pH. Before each measurement, the 0.1 M KOH electrolyte was bubbled with O_2 for more than 30 min.

The Koutecky-Levich plots can be analyzed for determining the electron transfer number (n) at various electrode potentials.

$$\frac{1}{j} = \frac{1}{j_k} + \frac{1}{B\omega^{1/2}} \quad (1)$$

$$B = 0.2nF(D_{O_2})^{2/3}\nu^{-1/6}C_{O_2} \quad (2)$$

Where j_k is the kinetic current, j is the measured current density, ω is the angular velocity of rotating electrode ($\omega = 2\pi N$, N is the linear rotation speed), F is the Faraday constant (96485 C mol^{-1}), C_{O_2} is the bulk concentration of O_2 (1.2×10^{-6} mol cm^{-3}), D_{O_2} is the diffusion coefficient of O_2 (1.9×10^{-5} cm^2 s^{-1}), and ν is the kinematic viscosity of the electrolyte (0.01 cm^2 s^{-1}) in 0.1 M KOH electrolyte.

$$n = \frac{4 \times i_d}{i_d + \frac{i_r}{N}} \quad (3)$$

$$HO_2^-\% = \frac{200 \times \frac{i_r}{N}}{i_d + \frac{i_r}{N}} \quad (4)$$

Where n is the electron transfer number, i_d is the disk current, i_r is the ring current and N is the current collection efficiency (0.37) of the Pt ring of RRDE electrode.[44]

Zn-air battery performance tests.

Aqueous Zn–Air Batteries Assembly: A graphical illustration of the home-made Zn-air battery is shown in Figure 5a. The polished Zn plate served as anode and the catalysts loaded on the nickel foam used as the air electrodes (cathode). The 6.0 M KOH electrolyte was filled between the cathode and anode. The catalyst ink prepared as described in the electrochemical measurements section was uniformly drop-cast the nickel foam to achieve a catalyst loading of 3.11 mg cm^{-2}.

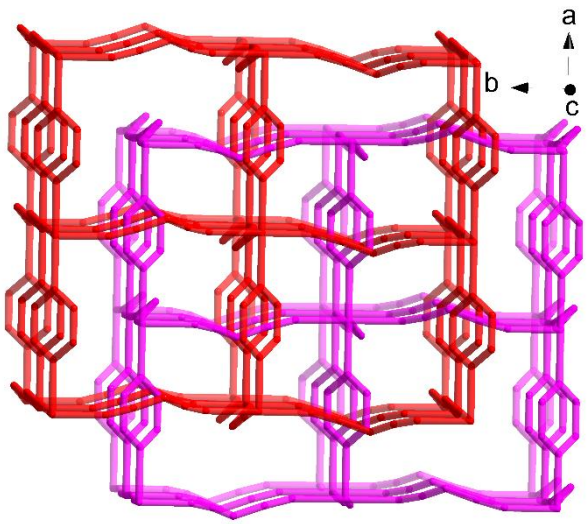

Figure S1. The two interpenetrating related networks of $Co(dca)_2pyz$.

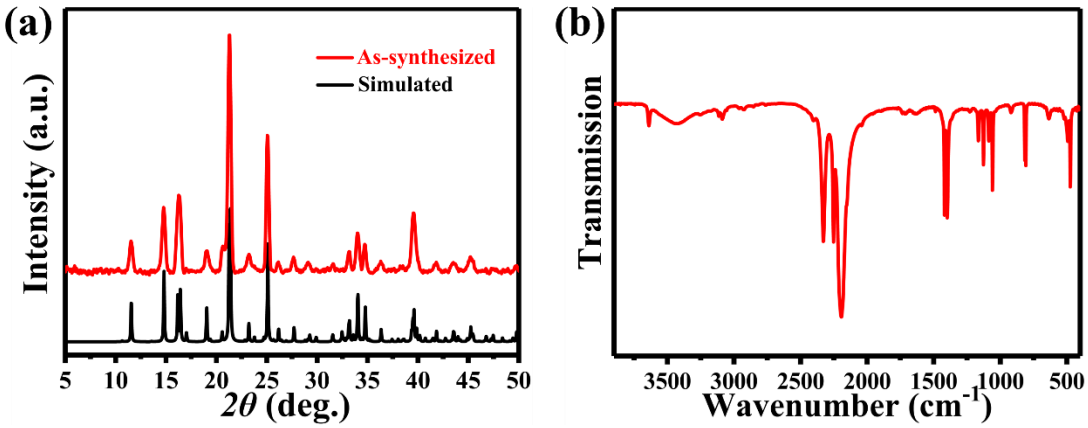

Figure S2. (a) PXRD pattern of the as-synthesized $Co(dca)_2pyz$ (Simulated pattern is obtained from the single crystal data by the Mercury 1.8, CCDC number: 153152).(b) The FTIR spectroscopy of $Co(dca)_2pyz$.

Table S1. Results of elemental analysis for the $Co(dca)_2pyz$ samples (obs.) compared with the theoretical values (calc.) and with reported data (Ref. 35).

Sample		C (%)	H (%)	N (%)
	Ref. 35	35.2	0.8	41.3
$Co(dca)_2pyz$	Obs.	35.2	1.4	41.3
	Calc.	35.4	1.5	41.3

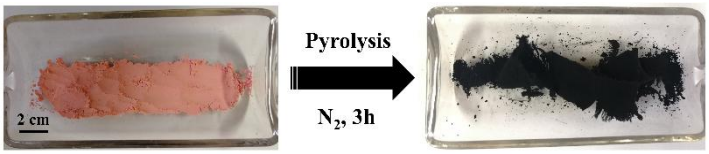

Figure S3. Photographs demonstration for the preparation of Co@BNCNTs.

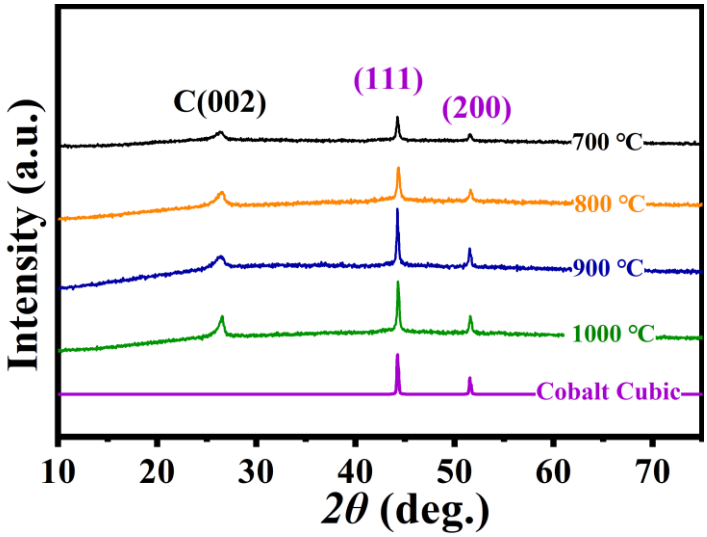

Figure S4. PXRD patterns for the Co@BNCNTs-700, 800, 900, 1000 materials compared to the simulated pattern of cubic cobalt.

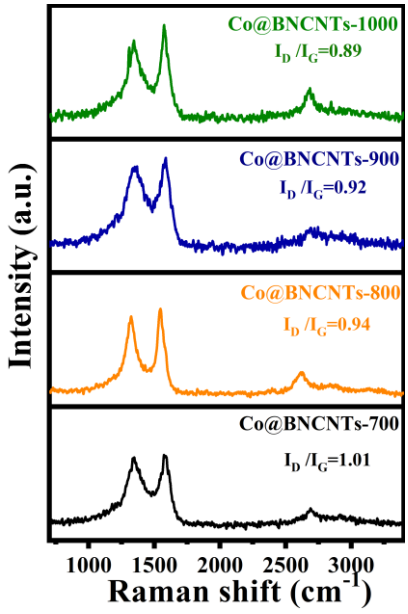

Figure S5. Raman spectra of the Co@BNCNTs catalysts.

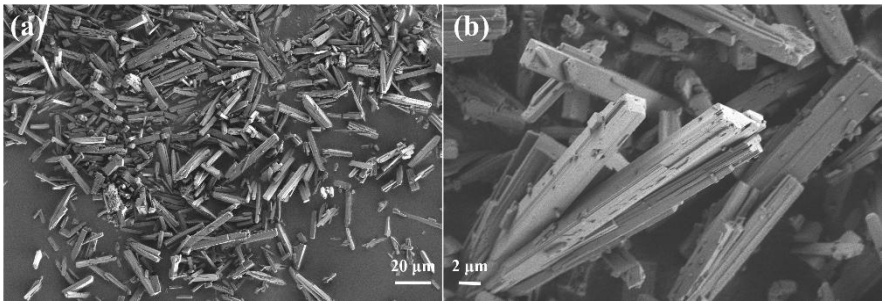

Figure S6. SEM images of the as-synthesized $Co(dca)_2pyz$.

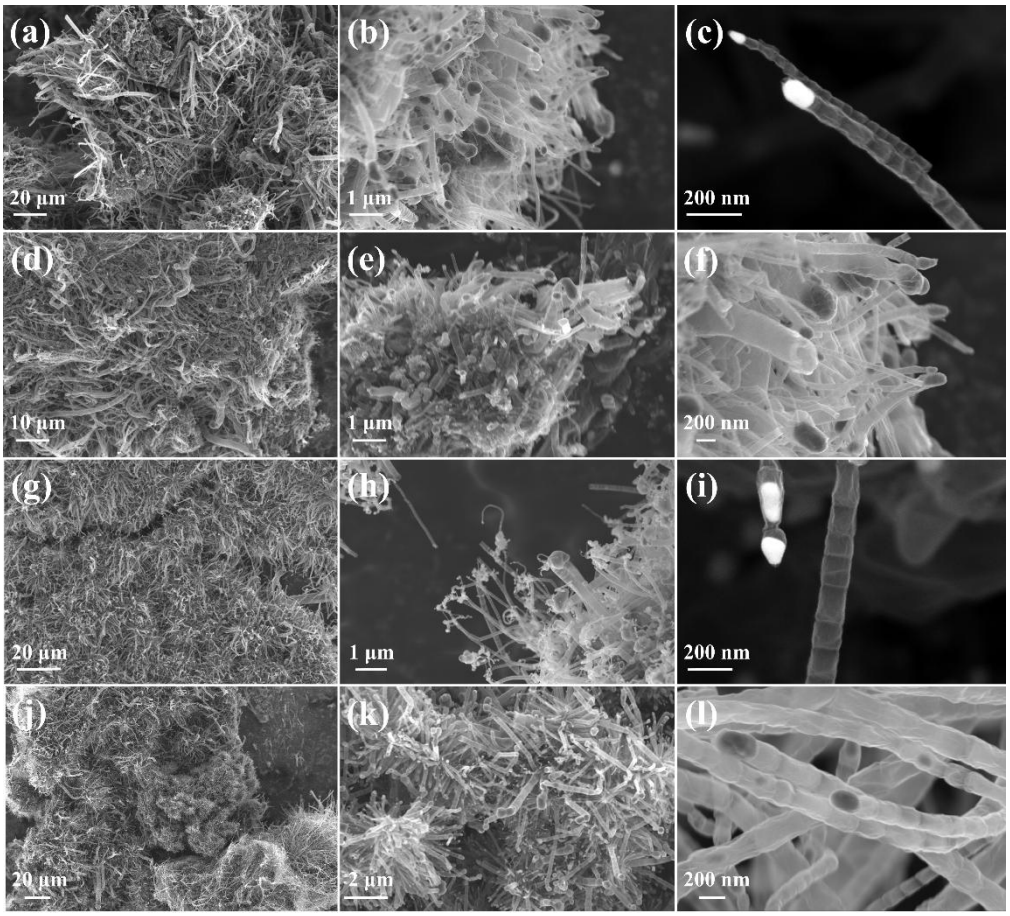

Figure S7. The SEM images of (a, b, c) Co@BNCNTs-700; (d, e, f) Co@BNCNTs-800; (g, h, i) Co@BNCNTs-900; (j, k, l) Co@BNCNTs-1000 materials derived from the Co-MOF.

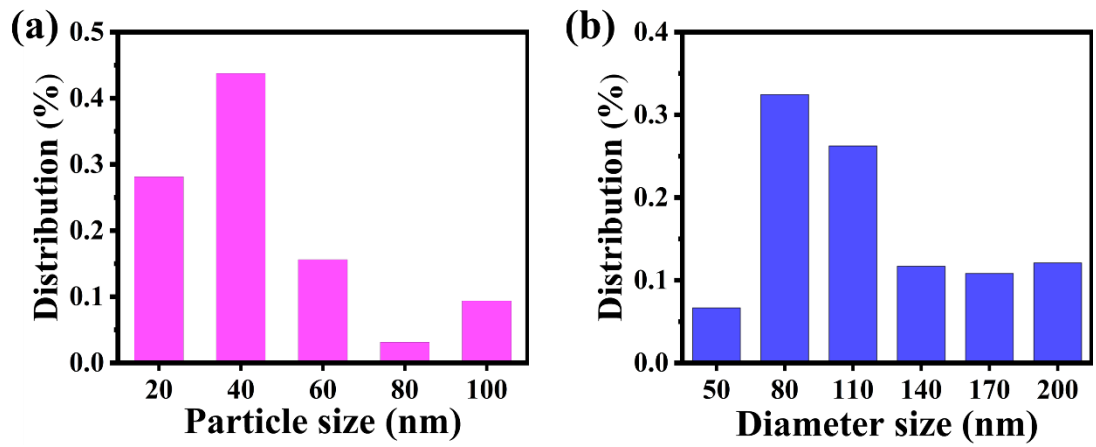

Figure S8. The statistical size distribution of (a) Co nanoparticles and (b) carbon nanotubes diameters from electron microscope images.

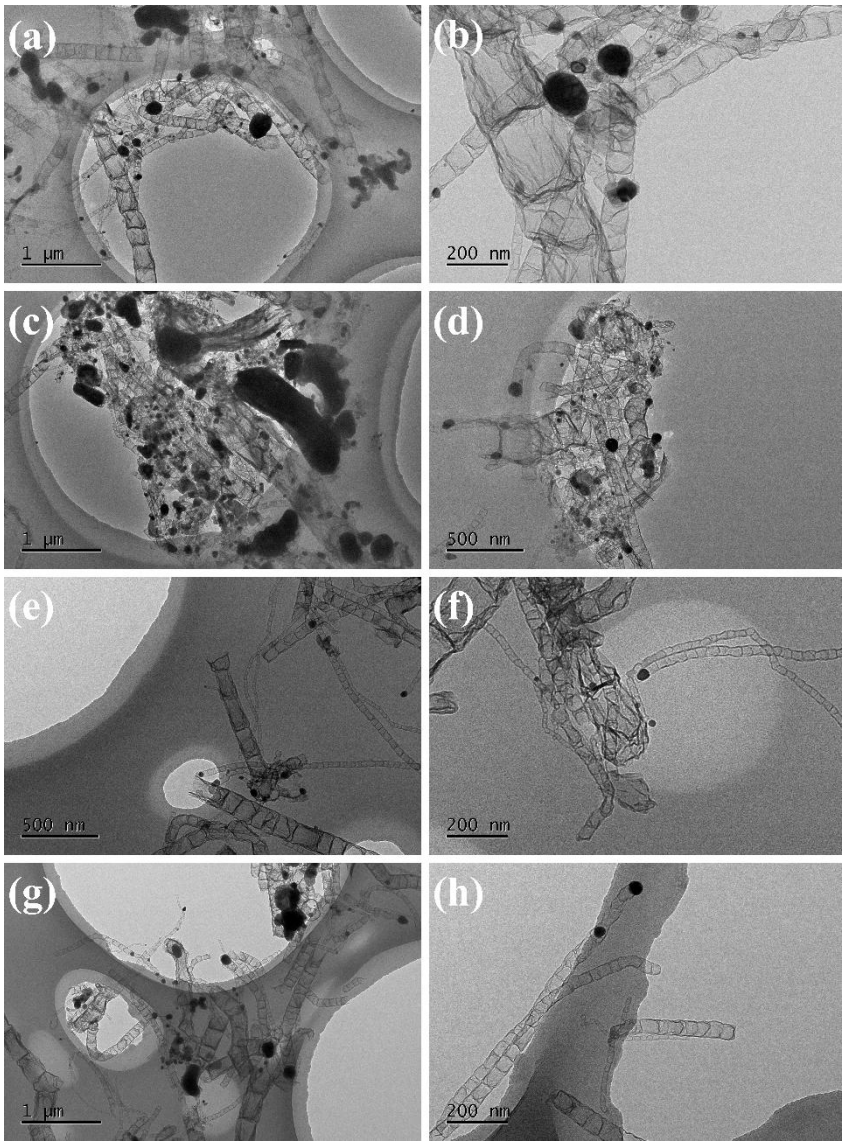

Figure S9. The TEM images of (a, b) Co@BNCNTs-700; (c, d) Co@BNCNTs-800; (e, f) Co@BNCNTs-900; (g, h) Co@BNCNTs-1000.

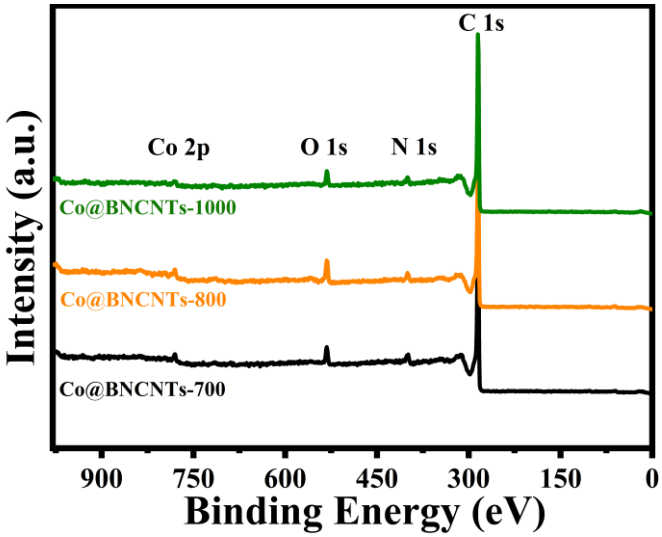

Figure S10. The XPS survey spectrum of Co@BNCNTs-700/800/1000 catalysts.

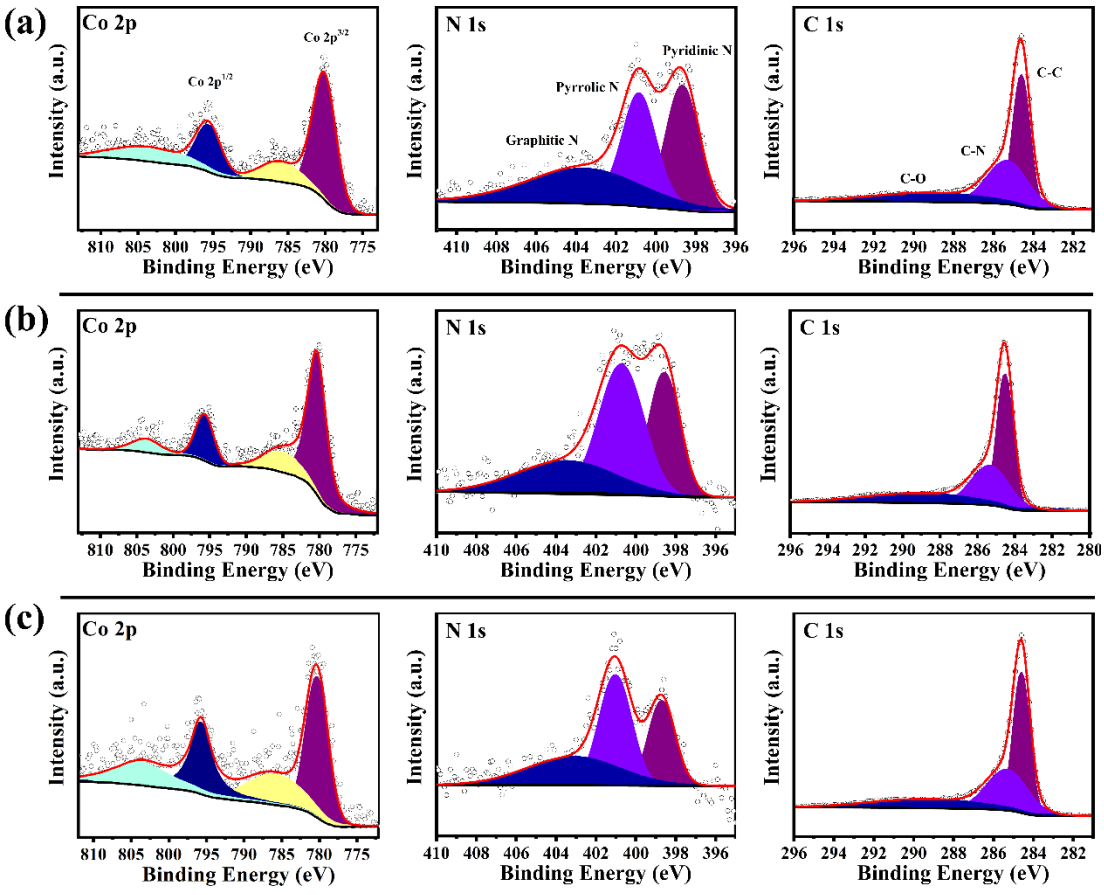

Figure S11. The XPS survey spectrum and high-resolution XPS spectra of the (a) Co@BNCNTs-700, (b) Co@BNCNTs-800 and (c) Co@BNCNTs-1000 catalyst for Co 2p, N 1s, C 1s respectively.

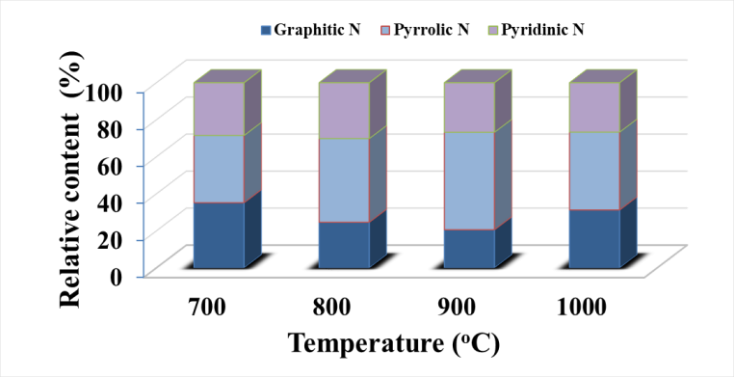

Figure S12. The total pyridinic N, pyrrolic N and graphitic N contents obtained from XPS.

Table S2. C/H/N elemental analysis results of different electrocatalysts (wt %).

Sample	C (%)	N (%)	H (%)
Co@BNCNTs-700	73.05	2.67	0.17
Co@BNCNTs-800	77.66	2.01	0.22
Co@BNCNTs-900	79.97	1.63	0.16
Co@BNCNTs-1000	79.92	1.25	0.14

Table S3. The surface elemental contents of Co@BNCNTs from XPS.

Sample	Co (At.%)	C (At.%)	N (At.%)	O (At.%)
Co@BNCNTs-700	0.55	92.03	5.35	2.08
Co@BNCNTs-800	0.7	91.29	3.11	3.11
Co@BNCNTs-900	0.45	92.83	2.09	4.62
Co@BNCNTs-1000	0.37	92.78	1.93	4.92

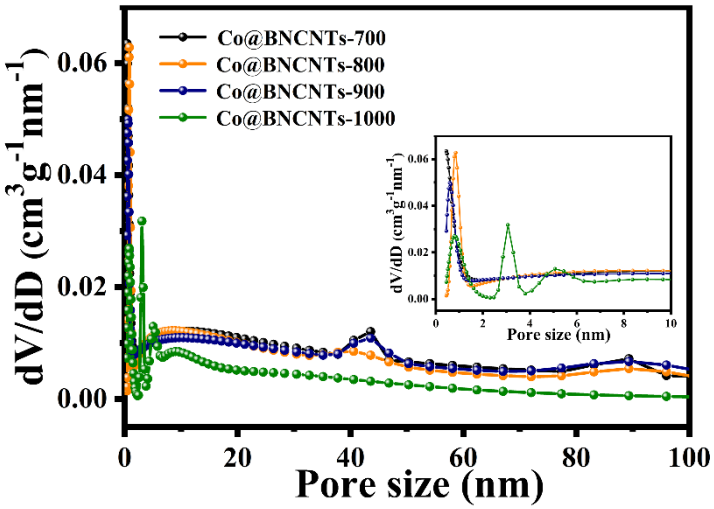

Figure S13. Pore size distributions calculated by using non-local density function theory (NLDFT) method for Co@BNCNTs catalysts.

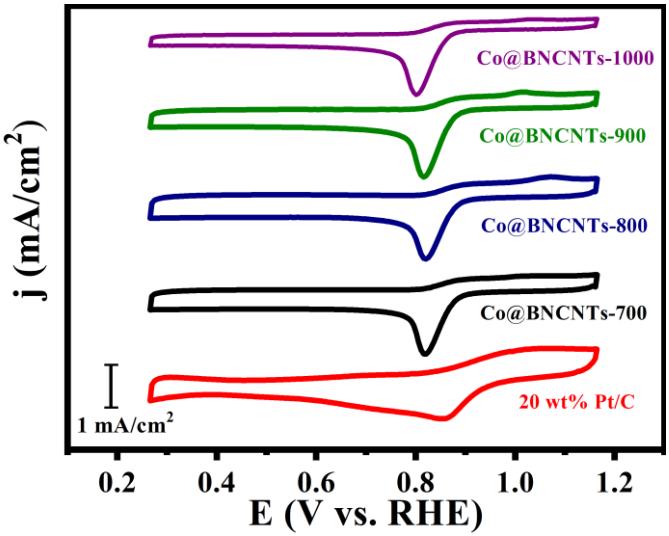

Figure S14. Cyclic voltammograms recorded for Co@BNCNTs-1000, 900, 800,700 and 20 wt% Pt/C in 0.1 M O_2-saturated KOH solution (scan rate: 20 mV s^{-1}).

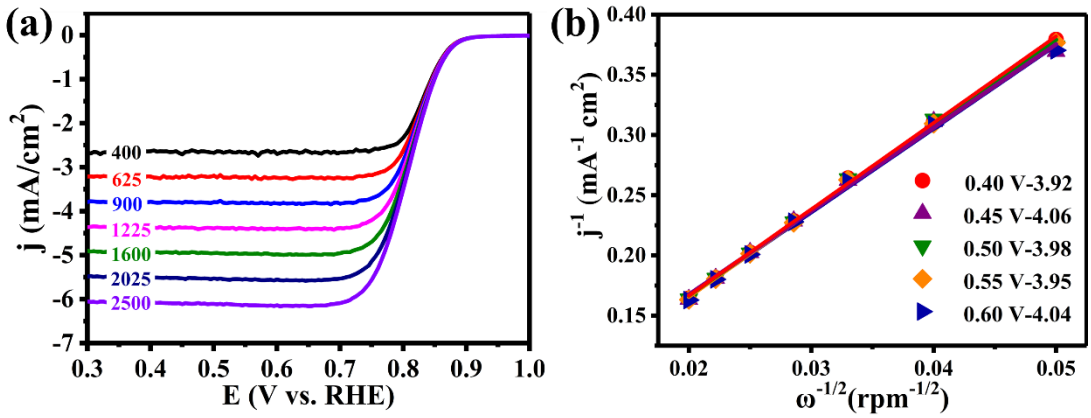

Figure S15. (a) ORR polarization curves at different rotating speeds and (b) the corresponding K–L plots and electron transfer number (n) at different potentials of the Co@BNCNTs-700.

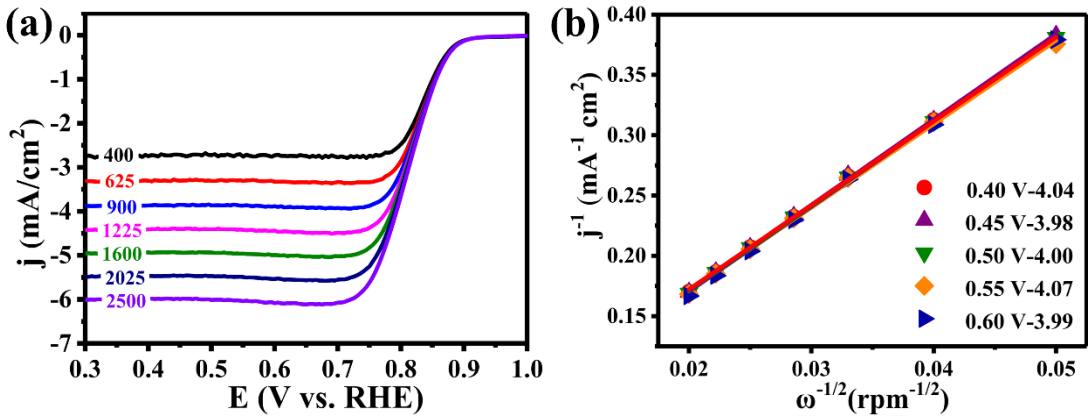

Figure S16. (a) ORR polarization curves at different rotating speeds and (b) the corresponding K–L plots and electron transfer number (n) at different potentials of the Co@BNCNTs-800.

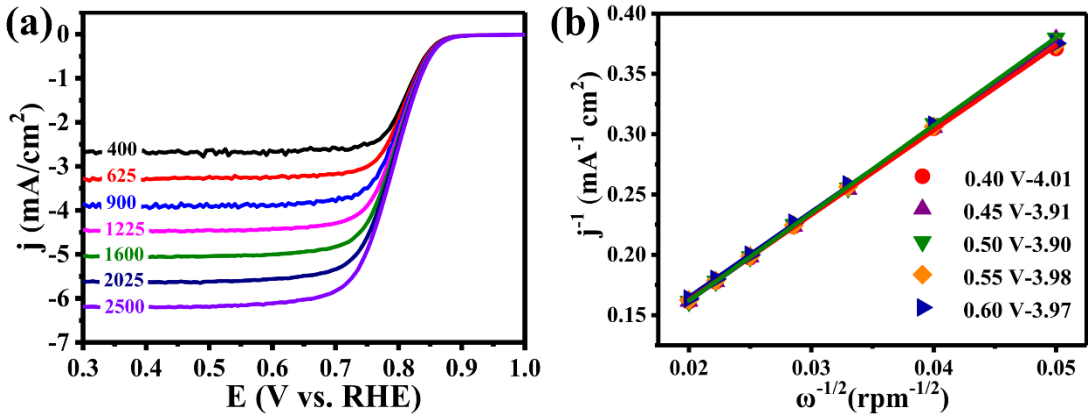

Figure S17. (a) ORR polarization curves at different rotating speeds and (b) the corresponding K–L plots and electron transfer number (n) at different potentials of the Co@BNCNTs-1000.

Table S4. Comparison of ORR catalytic performances in alkaline solution for Co@BNCNTs.

Sample	Half-wave Potential (V vs. RHE)	Onset Potential (V vs. RHE)	Diffusion Limiting Current Density ($mA\ cm^{-2}$)
Co@BNCNTs-700	0.81	0.91	4.90
Co@BNCNTs-800	0.81	0.91	4.95
Co@BNCNTs-900	0.82	0.93	5.31
Co@BNCNTs-1000	0.80	0.90	5.03

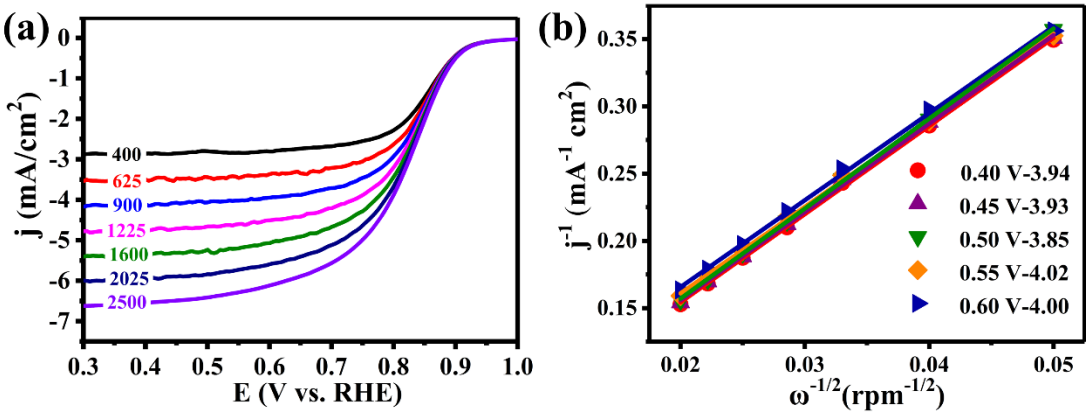

Figure S18. (a) ORR polarization curves at different rotating speeds and (b) the corresponding K–L plots and electron transfer number (n) at different potentials of the Pt/C.

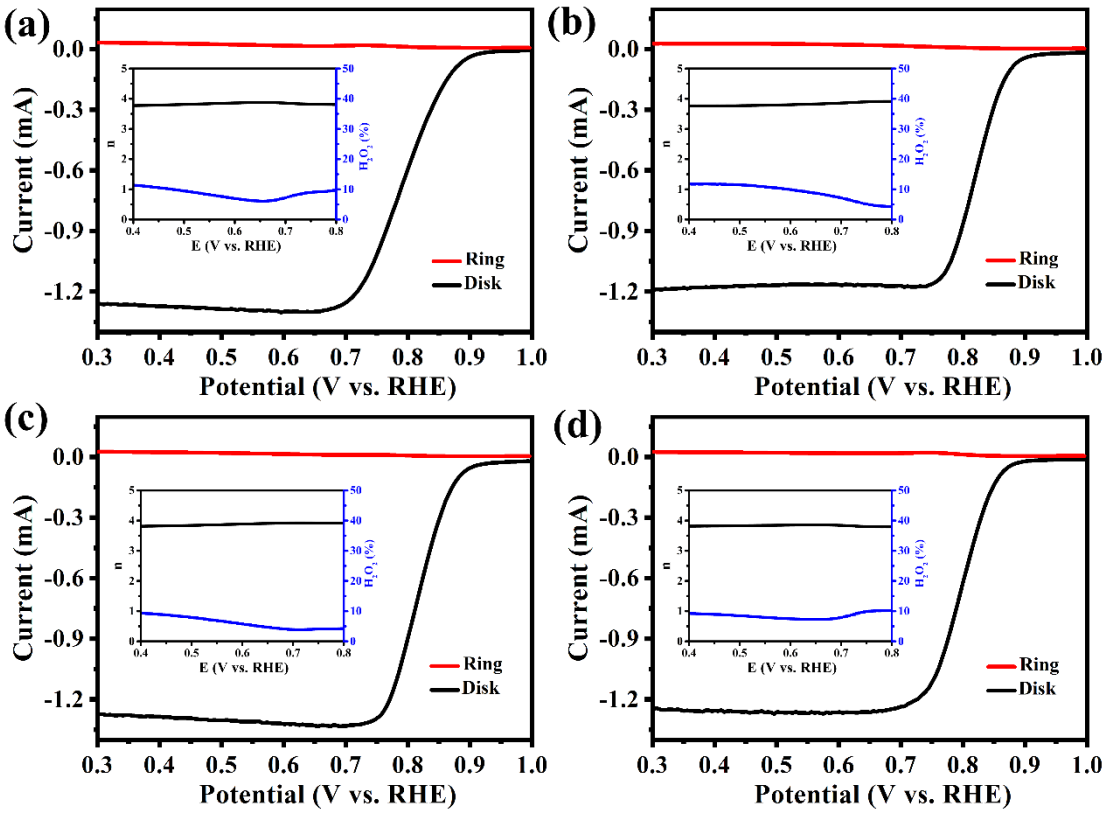

Figure S19. RRDE curve for (a) Co@BNCNTs-700, (a) Co@BNCNTs-800, (c) Co@BNCNTs-900 and (d) Co@BNCNTs-1000 at 1600 rpm. Inset: Peroxide yield and electron transfer number at various potentials.

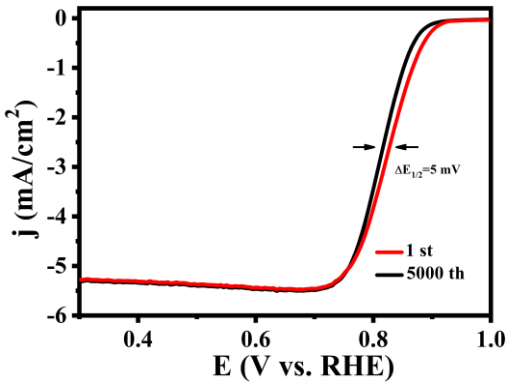

Figure S20. Endurance test of the Co@BNCNTs-900 catalyst after 5000 cycles in O_2-saturated 0.1 M KOH solution.

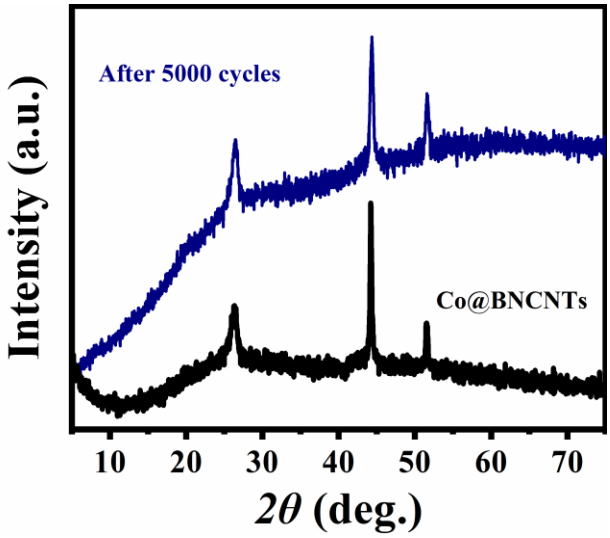

Figure S21. PXRD of the Co@BNCNTs-900 materials after accelerated stress test for 5000 cycles.

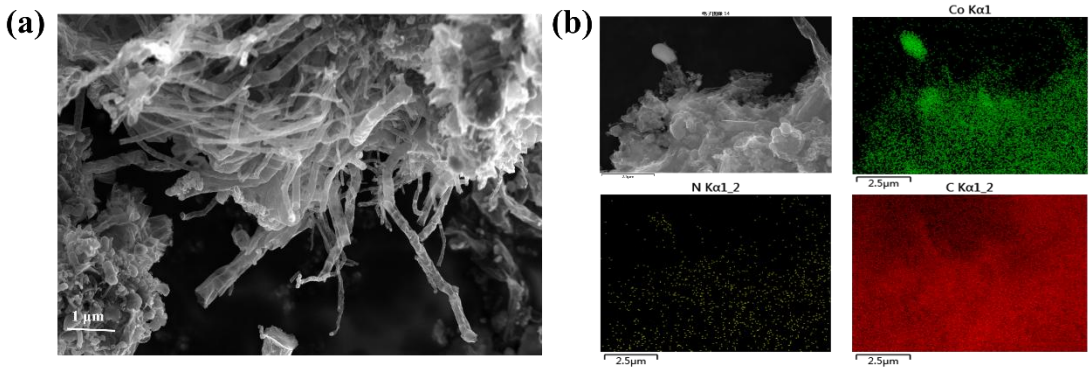

Figure S22. (a) SEM image and (b) corresponding elemental mappings of the Co@BNCNTs-900 after the long-term cycles.

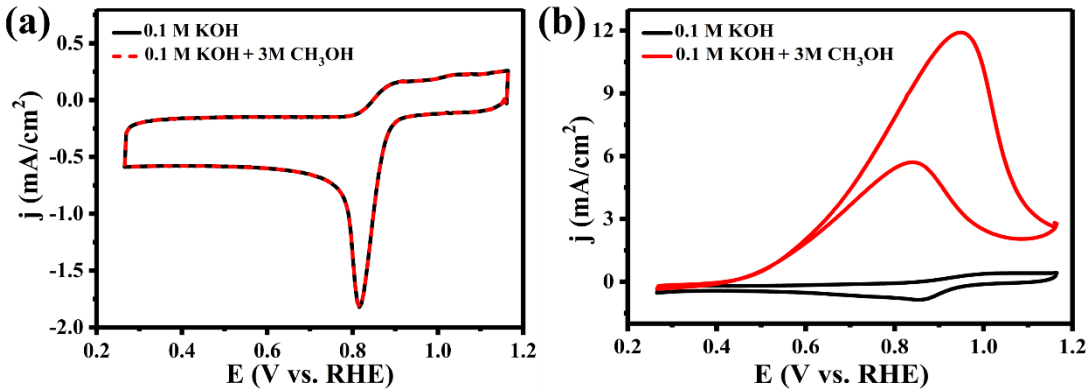

Figure S23. CV curves of (a) Co@BNCNTs-900 and (b) Pt/C in O_2-saturated 0.1 M KOH electrolyte with (red) or without (black) the addition of 3 M CH_3OH at a scan rate of 20 mVs^{-1}.

Table S5. A summary of synthetic methods for TM/CNTs.

Sample	Precursor	Preparation condition			Ref
		Temperature	Atmosphere	Time	
Co/N-CNTs @$Ti_3C_2T_x$	Ti, Al, C $Co(NO_3)_2$ Dicyandiamide	Step 1: 1400 ℃ Step 2: 900 ℃	Ar N_2	2 h 60 min	S1
Co/N-BCNTs	Urea Zn/Co-ZIF	Step 1: 550 ℃ Step 2: 900 ℃	– N_2	4 h 1 h	8
CoNi@NCNT/NF	Nickel foam Melamine $Co(NO_3)_2$	Step 1: – Step 2: 700 ℃	Air N_2	– 1 h	9
3D-CNTA	ZIF-67 Melamine	Step 1: 550 ℃ Step 2: 650-900 ℃	N_2	3 h 3 h	11
N-GCNT/FeCo	$Co(NO_3)_2$ $Fe(NO_3)_3$ Glutamic acid Melamine	Step 1: 500 ℃ Step 2: 800 ℃	N_2	– 2 h	S2
Fe_3C@NCNT/NP	Fe-MIL-88B Melamine	Step 1: 550 ℃ Step 2: 700-900 ℃	N_2	3 h 2 h	17
Co@NCNT	ZIF-67 Dicyandiamide	Step 1: 500 ℃ Step 2: 650-850 ℃	– Ar	30 min 3 h	18
Co-NRCNTs	Dicyandiamide $CoCl_2$	Step 1: 500 ℃ Step 2: 700-900 ℃	N_2	2 h 2 h	22
Co@NCNTs	ZIF-67	Step 1: 350 ℃ Step 2: 700 ℃	Ar/H_2	1 h 4 h	S3
NCNTFs	ZIF-67	One step: 700 ℃	Ar/H_2	3.5 h	19
N-CNT	ZIF-67	One step: 435 ℃	Ar	8 h	34
NCNT	CoAl-LDH ZIF-67	One step: 800 ℃	H_2	2 h	15
Co@NC-x/y	Co_xZn_y-BMZIF	One step: 900 ℃	Ar	2 h	12
Co-NCNT/NP	ZnCo-ZIFs	One step: 800 ℃	Ar/H_2	3 h	16
Co-NC/CNT	ZIF-67 CNT	One step: 700-900 ℃	N_2	2 h	S4
Co-C/CNT	ZIF-67	One step: 900 ℃	N_2	10 h	S5
Co@BNCNTs	**Dicyanamide-based Co-MOF**	**One step: 700-1000 ℃**	**N_2**	**3 h**	**This work**

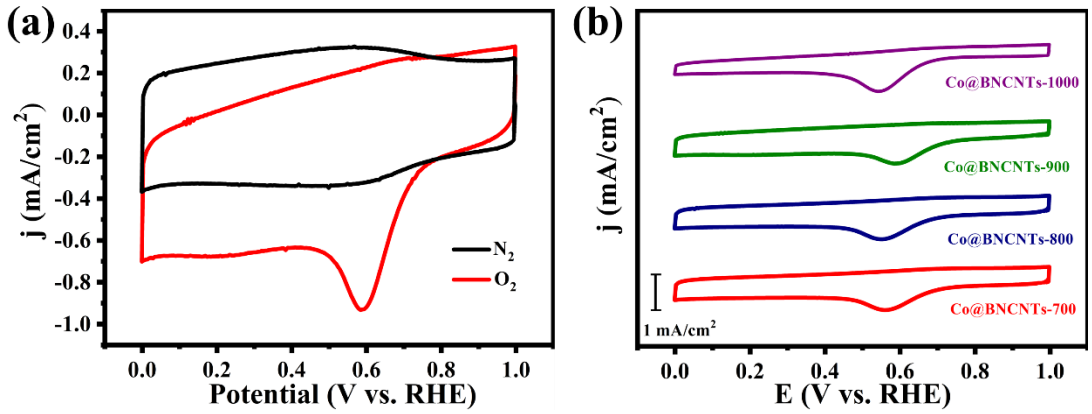

Figure S24. CV curves of (a)Co@BNCNTs-900 in O_2- and N_2-saturated electrolyte and (b) four samples in 0.1M O_2-saturated $HClO_4$ (scan rate: 20 mV s^{-1}).

Note: Featureless voltammetric currents were observed for all samples in N_2, while they displayed well-defined cathodic peaks in O_2, which confirm their catalytic activities for the ORR.

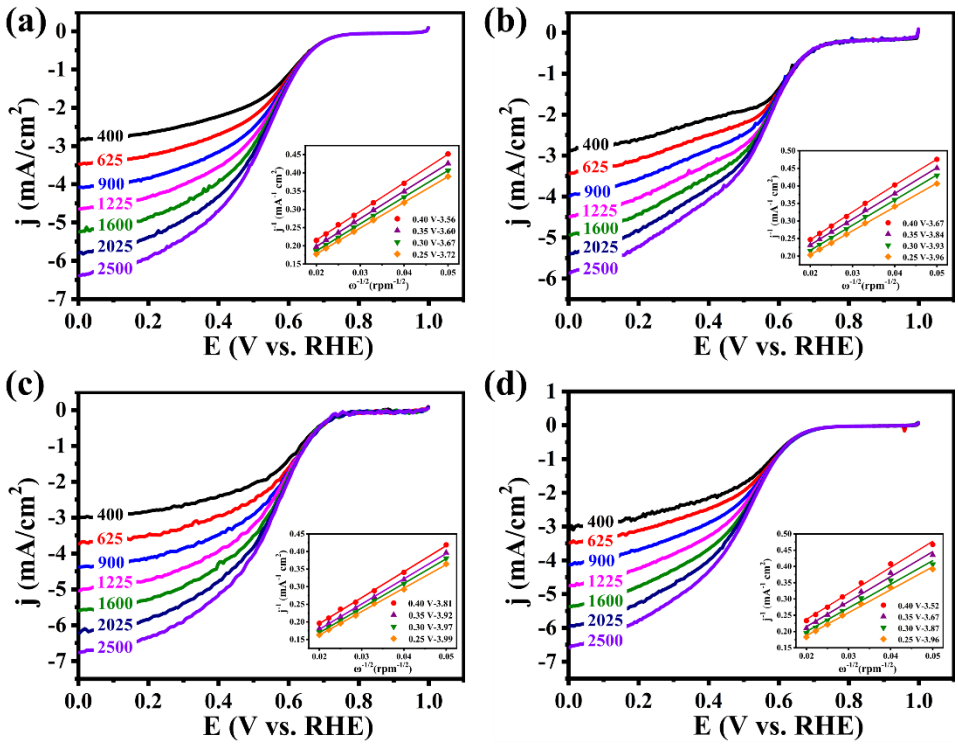

Figure S25. ORR polarization curves at different rotating speeds for (a) Co@BNCNTs-700, (b) Co@BNCNTs-800, (c) Co@BNCNTs-900, (d) Co@BNCNTs-1000 in 0.1 M O_2-saturated $HClO_4$ solution (scan rate: 5 mV s^{-1}). Inset: the corresponding K–L plots and electron transfer numbers at different potentials.

Note: Here, the Co@BNCNTs-900 showed the highest electron transfer number with an average value of 3.90 in the potential range of 0.25–0.40 V, implying a dominant four-electron pathway.

Table S6. Comparison of ORR catalytic performances in acidic solution for Co@BNCNTs.

Sample	Half-wave Potential (V vs. RHE)	Onset Potential (V vs. RHE)	Diffusion Limiting Current Density (mA cm^{-2})
Co@BNCNTs-700	0.50	0.74	5.24
Co@BNCNTs-800	0.53	0.74	5.0
Co@BNCNTs-900	0.55	0.75	5.60
Co@BNCNTs-1000	0.49	0.72	5.34

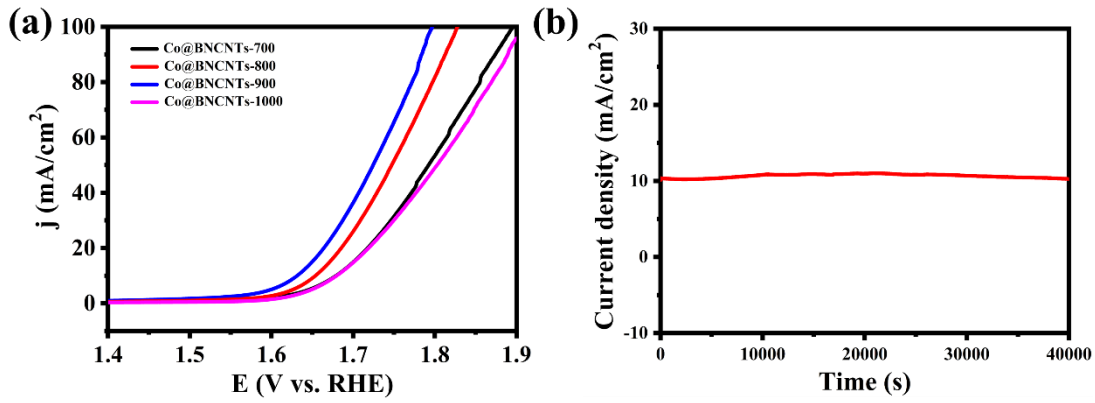

Figure S26. (a) LSV plots of different catalysts measured in 1 M KOH electrolyte; (b) The chronoamperometric measurements of Co@BNCNTs-900.

Note: Here, the polarization curve of Co@BNCNTs-900 achieves the current density of 10 mA cm^{-2} at an overpotential of 400 mV and the chronoamperometry test for Co@BNCNTs-900 at a constant potential of 1.63 V reveals the stability of the material.

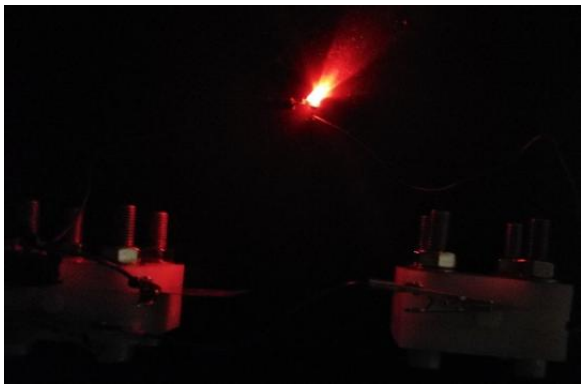

Figure S27. Red LED powered by two-series batteries in the darkroom.

Table S7. Comparison of ORR performance of Co@BNCNTs with other non-precious metal-based catalysts.

Sample	**CV peak potential (V)**	**Onset Potential (V vs. RHE)**	**Half-wave Potential (V vs. RHE)**	**Loading (mg cm^{-2})**	**Ref**
Co/N-CNTs@Ti_3C_2Tx	0.80	0.936	0.815	0.408	S1
Co/N-BCNTs	0.80	–	0.83	0.2	8
NCNT	–	0.825	0.812	0.2	15
Co@NCNT	0.814	1.03	0.828	–	18
Co–CNT/PC	0.831	0.918	–	0.152	21
Co_3O_4@C-MWCNTs	0.79	0.89	0.81	0.325	30
Co/CoP–HNC	–	0.94	0.83	0.19	23
N,S-NH_3-C-7	0.78	–	0.83	0.1	4
N-CNTs-650	0.87	0.94	0.85	–	34
DCI-Fe-700	0.785	–	0.813	0.1	S6
MnO_2 nanorods	0.77	0.90	0.76	–	S7
Co@BNCNTs	**0.83**	**0.93**	**0.82**	**0.3**	**This work**

Table S8. Comparison of Zn-air battery performance of Co@BNCNTs with other state-of-the-art electrode materials.

Sample	**Open-circuit potential (V)**	**Peak power density (mW cm^{-2})**	**Current density at 1.0 V (mA cm^{-2})**	**Cycle hour (h)**	**Ref**
Co_3O_4/NHPC	–	80	59	7.5	S8
Co@NPC-acid	1.39	78.75	40	–	S9
Mn oxide/XC72	1.44	67.51	40	–	S10
NPMC-1000	1.48	55	–	30	S11
$CuCo_2O_4$/N-CNTs	1.36	83.83	50	48	13
Cu_3P@NPPC	1.46	110.8	–	35	44
Co–CNT/PC	1.37	–	–	16.6	21
FeNi@N-GR	1.48	85	59	18	S12
Co@BNCNTs	**1.48**	**90**	**55**	**65**	**This work**

References

[S1] Y. Zhang, H. Jiang, Y. Lin, H. Liu, Q. He, C. Wu, T. Duan and L. Song, *Adv. Mater. Interfaces*, 2018, **5**, 1800392.

[S2] C.-Y. Su, H. Cheng, W. Li, Z.-Q. Liu, N. Li, Z. Hou, F.-Q. Bai, H.-X. Zhang and T.-Y. Ma, *Adv. Energy Mater*., 2017, **7**, 1602420.

[S3] J.-S. Li, B. Du, Z.-H. Lu, Q.-T. Meng and J.-Q. Sha, *New J. Chem*., 2017, **41**, 10966-10971.

[S4] F. Yang, P. Zhao, X. Hua, W. Luo, G. Cheng, W. Xing and S. Chen, *J. Mater. Chem. A*, 2016, **4**, 16057-16063.

[S5] Y. Ma, Y. Ma, D. Bresser, Y. Ji, D. Geiger, U. Kaiser, C. Streb, A. Varzi and S. Passerini, *ACS Nano*, 2018, **12**, 7220-7231.

[S6] Z. Li, H. Sun, L. Wei, W.-J. Jiang, M. Wu and J.-S. Hu, *ACS Appl. Mater. Interfaces*, 2017, **9**, 5272-5278.

[S7] T. Zhang, F. Cheng, J. Du, Y. Hu and J. Chen, *Adv. Energy Mater.*, 2014, **5**, 1400654.

[S8] J. Guan, Z. Zhang, J. Ji, M. Dou and F. Wang, *ACS Appl. Mater. Interfaces*, 2017, **9**, 30662-30669.

[S9] H. Liu, M.-Q. Wang, Z.-Y. Chen, H. Chen, M.-W. Xu and S.-J. Bao, *Dalton Trans.*, 2017, **46**, 15646-15650.

[S10] P.-C. Li, C.-C. Hu, T.-C. Lee, W.-S. Chang and T. H. Wang, *J. Power Sources*, 2014, **269**, 88-97.

[S11] J. Zhang, Z. Zhao, Z. Xia and L. Dai, *Nat. Nanotechnol.*, 2015, **10**, 444.

[S12] L. Yang, X. Zeng, W. Wang and D. Cao, *Adv. Funct. Mater.*, 2017, **28**, 1704537.